COMPUTER METHODS AND PROGRAMS IN BIOMEDICINE 87 (2007) 46–60

journal homepage: www.intl.elsevierhealth.com/journals/cmpb

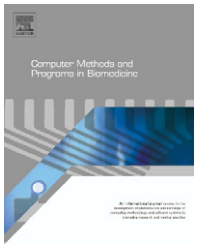

Model-based cardiac diagnosis of pulmonary embolism

C. Starfinger[a], *C.E. Hann*[a,*], *J.G. Chase*[a], *T. Desaive*[b], *A. Ghuysen*[c], *G.M. Shaw*[d]

[a] *Centre of Bioengineering, University of Canterbury, Christchurch, New Zealand*
[b] *Institute of Physics, University of Liège, Belgium*
[c] *Hemodynamics Research Laboratory, University of Liège, Belgium*
[d] *Department of Intensive Care Medicine, Christchurch Hospital, Christchurch, New Zealand*

ARTICLE INFO

Article history:
Received 21 August 2006
Received in revised form
14 February 2007
Accepted 18 March 2007

Keywords:
Cardiovascular system
Cardiac model
Parameter identification
Integral method
Pulmonary embolism

ABSTRACT

A minimal cardiac model has been shown to accurately capture a wide range of cardiovascular system dynamics commonly seen in the intensive care unit (ICU). However, standard parameter identification methods for this model are highly non-linear and non-convex, hindering real-time clinical application. An integral-based identification method that transforms the problem into a linear, convex problem, has been previously developed, but was only applied on continuous simulated data with random noise. This paper extends the method to handle discrete sets of clinical data, unmodelled dynamics, a significantly reduced data set theta requires only the minimum and maximum values of the pressure in the aorta, pulmonary artery and the volumes in the ventricles. The importance of integrals in the formulation for noise reduction is illustrated by demonstrating instability in the identification using simple derivative-based approaches. The cardiovascular system (CVS) model and parameter identification method are then clinically validated on porcine data for pulmonary embolism. Errors for the identified model are within 10% when re-simulated and compared to clinical data. All identified parameter trends match clinically expected changes. This work represents the first clinical validation of these models, methods and approach to cardiovascular diagnosis in critical care.

1. Introduction

Cardiac disease state is highly patient specific and difficult to accurately diagnose due to the limited measurements available. In addition, the body's natural reflex responses try to restore circulatory equilibrium, which can often mask the underlying symptoms [1,2]. Successful diagnosis and treatment often rely on the experience and intuition of clinical staff. Thus, a physiological, identifiable and validated computer model offers several potential advantages in diagnosis and therapy selection, by aggregating diverse patient data into a compact, patient specific, clinically relevant and potentially real-time assessment of circulatory status.

There are many CVS models in the literature ranging from very complex finite element models [3–6] to relatively simpler pressure volume approaches [7–9]. However, the focus is often on only specific areas of CVS dysfunction. Although there are full CVS models, patient-specific parameter optimization is either not considered or restricted to small subsets of the overall much larger parameter set (e.g.[10,11]). This restriction to specific CVS aspects can dramatically limit the range of CVS disturbances that can be detected, thus prohibiting use as a broader diagnostic tool for patients with unknown condition. For relatively larger, more complex system models computational cost and feasibility can also become a major issue.

* *Corresponding author*. Tel.: +64 3 366 7001; fax: +64 3 364 2078.
E-mail address: chris.hann@canterbury.ac.nz (C.E. Hann).
0169-2607/$ – see front matter © 2007 Elsevier Ireland Ltd. All rights reserved.
doi:10.1016/j.cmpb.2007.03.010

This research employs a physiologically validated minimal model [12–15] capable of capturing patient dynamics commonly seen in an ICU, while using a relatively small number of physiological variables. A highly efficient solution method [16] provides the necessary simplicity, flexibility and rapid forward simulation that is required in a clinical environment. An integral-based parameter identification method has been also been developed and shown, in simulation, to rapidly and accurately identify virtually the entire parameter set in the presence of significant measurement noise [17]. However, a relatively large measured data set was assumed, including continuously measured pressure and flow waveforms. Such measurements might not always be clinically available.

In this paper, the integral method is extended to allow discrete sets of clinical data and is shown to be robust to unmodelled dynamics and measurement noise. The measurements utilized are also reduced from prior work to a more clinically feasible set. The use of integrals in the formulation is shown to be critical for stability, even with locally smoothed curves, as compared to numerical derivative-based identification approaches. The method is initially tested on simulations of pulmonary embolism that capture all the physiologically expected responses. The CVS model and integral method are then clinically validated on a porcine model of pulmonary embolism.

2. Methodology

2.1. CVS model

The CVS model is a lumped parameter model [19], where the left and right ventricle chambers are characterized by the flow in and out of the chamber, the pressure up- and downstream and the resistances of the valves, and inertia of the blood. An overview of the model is given in Fig. 1. To add flexibility and better match waveform shape as well as peak values, the model is extended from [19] to allow a slightly non-linear pressure–volume relationship in the aorta and pulmonary artery. The equations for the left ventricle are defined:

$$V_{pcd} = V_{lv} + V_{rv} \tag{1}$$

$$P_{pcd} = P_{0pcd} \cdot (e^{\lambda_{pcd}(V_{pcd} - V_{0pcd})} - 1) \tag{2}$$

$$P_{peri} = P_{pcd} + P_{th} \tag{3}$$

$$V_{lvf} = V_{lv} - V_{spt} \tag{4}$$

$$P_{lvf} = \mathrm{dri}L \cdot E_{eslvf} \cdot V_{lvf} + (1 - \mathrm{dri}L) \cdot P_{0lvf} \cdot (e^{\lambda_{lvf} V_{lvf}} - 1) \tag{5}$$

$$P_{lv} = P_{lvf} + P_{peri} \tag{6}$$

$$P_{pu} = E_{pu} \cdot V_{pu} + P_{th} \tag{7}$$

$$\dot{V}_{ao} = Q_{av} - Q_{sys} \tag{8}$$

$$Q_{sys} = \frac{P_{ao} - P_{vc}}{R_{sys}} \tag{9}$$

$$P_{ao} = E_{ao} \cdot V_{ao}^{f} \tag{10}$$

$$\dot{V}_{lv} = Q_{av} - Q_{mt} \tag{11}$$

$$\dot{Q}_{mt} = H(H(P_{pu} - P_{lv}) + H(Q_{mt})) \cdot \frac{(P_{pu} - P_{lv} - R_{mt} \cdot Q_{mt})}{L_{mt}} \tag{12}$$

$$\dot{Q}_{av} = H(H(P_{lv} - P_{ao}) + H(Q_{av})) \cdot \frac{(P_{lv} - P_{ao} - R_{av} \cdot Q_{av})}{L_{av}} \tag{13}$$

where H is the Heaviside function, f is a non-linear factor ranging from 0.8 to 1.4, and all other variables are as shown in Fig. 1. Similar equations are used for the right ventricle and pulmonary/systemic circulation. For a more detailed description see [19,16,12–14]. The parameter f in Eq. (10) provides more flexibility to capture the shape and peak of P_{ao} seen in clinical data. Definitions of the parameters in the model are given in Table 1.

2.1.1. Activation function

The electrical activation of the left and right ventricles are described using a driver function and time varying elastance to model cardiac muscle activation [19,7]. For clinical validation on the porcine data, separate driver functions are chosen for the left and right ventricles:

$$\mathrm{dri}_L = A_L \cdot e^{(-b_L \cdot (t - (\mathrm{period}/c_L))^2)} \tag{14}$$

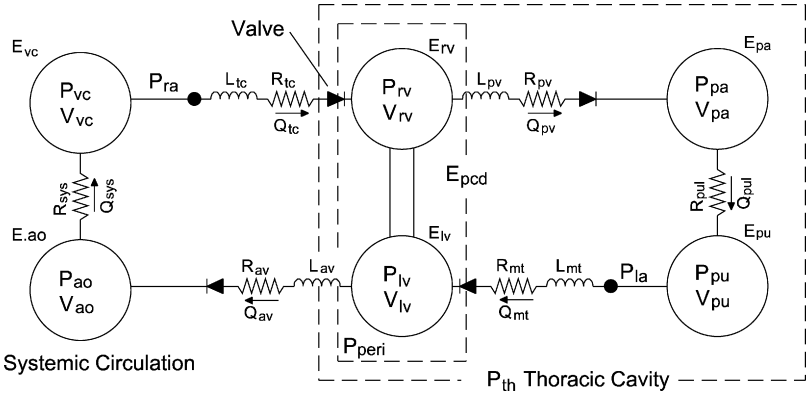

Fig. 1 – Minimal CVS model overview. The model is made up of elastic chambers connected by resistors and conductors in series. Each elastic chamber simulates the pressure–volume relationship in a particular area of the circulation.

Table 1 – Abbreviations used in CVS model

Abbreviation	Description
λ	Parameter in EDPVR
P_0	Parameter in EDPVR
lv	Left ventricle
rv	Right ventricle
lvf	Left ventricle free wall
rvf	Right ventricle free wall
spt	Septum
pcd	Pericardium
V_0	Volume at zero pressure
V_d	Unstressed chamber volume
R	Resistance
E	Elastance
L	Inertance
P	Pressure
Q	Flow
V	Volume
mt	Mitral valve
tc	Tricuspid valve
av	Aortic valve
pv	Pulmonary valve
pul	Pulmonary
sys	Systemic
es	End-systolic
P_{ao0}	Initial pressure ($P_{ao}(0)$) in arta
P_{pa0}	Initial pressure ($P_{pa}(0)$) in pulmonary artery
P_{vc0}	Initial pressure ($P_{vc}(0)$) in vena cava
P_{pu0}	Initial pressure ($P_{pu}(0)$) in pulmonary vein
P_{th}	Intrathoracic pressure
EDPVR	End-diastolic pressure–volume relationship
ESPVR	End-systolic pressure–volume relationship
period	Heartbeat period

$$\mathrm{dri}_R = A_R \cdot e^{(-b_R \cdot (t-(\mathrm{period}/c_R))^4)} \tag{15}$$

$$\mathrm{period} = \frac{1}{\mathrm{heartrate}} \tag{16}$$

where $A_L = 1$, $b_L = 2582.177$, $c_L = 2.07$ and $A_R = 1$, $b_R = 91.5975$, $c_R = 2.18$ for the left (L) and right ventricles (R). The drivers are shown in Fig. 2 for a period of 0.53 s, and are developed from scaling pressures for the porcine data.

The use of two different driver functions is physiologically justified, as the electric signal spreads differently in both ventricles. More specifically, the cardiac activation pattern and times have been clinically observed to differ between the right and left ventricles [20,21]. The activation function is also defined to change as a function of the heart period.

For human simulations the same driver function is used for both ventricles and the septum volume, and is defined [7,19]:

$$\mathrm{dri} = 1 \cdot e^{(-80 \cdot (t-(\mathrm{period}/2))^2)} \tag{17}$$

Only one driver function is used mainly for simplicity, and for an initial proof of concept on human parameters. However, note that for humans, in practice, the pressure–volume relationship in the right ventricle is very difficult to measure and thus there is no readily available data to obtain a driver function. In the porcine case, the pressures in left and right ventricles were available, thus two different generic driver functions could be found. This enabled better matching to the overall waveform shapes of the output signals.

2.1.2. *Ventricular interaction*

Ventricular interaction is an important dynamic [22,23] and is included in the model. The septum volume is described by a time-varying P–V relationship defined [7,19,14]:

$$P_{spt} = \mathrm{dri}\,S \cdot E_{esspt}(V_{spt} - V_{dspt}) + (1 - \mathrm{dri}\,S) \cdot P_{0spt}(e^{\lambda_{spt}(V_{spt}-V_{0spt})} - 1) \tag{18}$$

where the driver function dri S describing the activation of the septum, is taken from [7,19,14]. The septum volume V_{spt} can be determined analytically using the methods in [17]:

$$V_{spt} = \frac{a}{b} \tag{19}$$

with a and b defined:

$$a = (\mathrm{dri}\,S \cdot E_{esspt} \cdot V_{dspt} + \mathrm{dri}\,L \cdot E_{eslvf} \cdot V_{lv} - \mathrm{dri}\,R \cdot E_{esrvf} \cdot V_{rv} - (1 - \mathrm{dri}\,S) \cdot P_{0spt} \cdot (b_{spt}\, e^{-\lambda_{spt} V_{0spt}} - 1) + (1 - \mathrm{dri}\,L) \cdot P_{0lvf} \cdot (b_{lvf}\, e^{\lambda_{lvf} V_{lv}} - 1) - (1 - \mathrm{dri}\,R) \cdot P_{0rvf} \cdot (b_{rvf}\, e^{\lambda_{rvf} V_{rv}} - 1)) \tag{20}$$

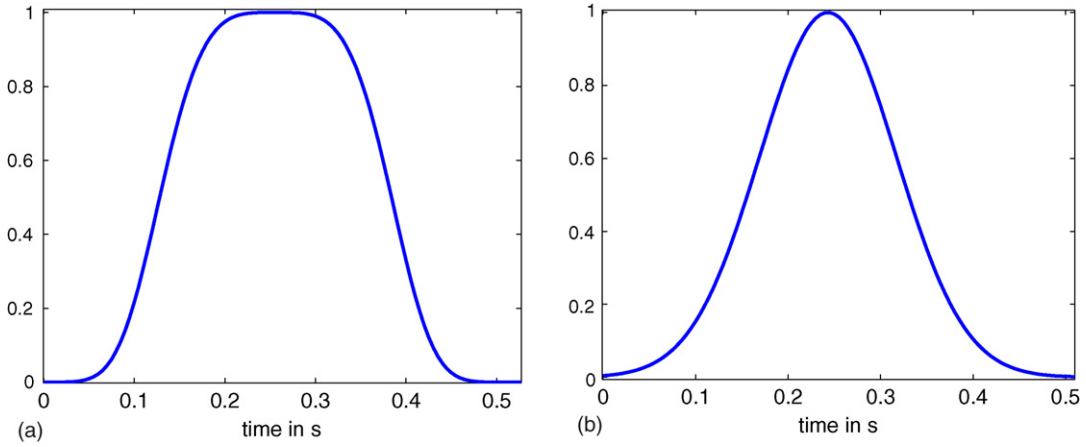

Fig. 2 – Driver functions for ventricle activation. The drivers are shown for a period of 0.53 s: (a) left ventricle; (b) right ventricle.

$$b = (\mathrm{dri}\,S \cdot E_{\mathrm{esspt}} - \mathrm{dri}\,L \cdot E_{\mathrm{eslvf}} - \mathrm{dri}\,R \cdot E_{\mathrm{esrvf}} + (1 - \mathrm{dri}\,S) \cdot P_{0\mathrm{spt}} \cdot a_{\mathrm{spt}}\, e^{-\lambda_{\mathrm{spt}} V_{0\mathrm{spt}}} - (1 - \mathrm{dri}\,L) \cdot P_{0\mathrm{lvf}} \cdot a_{\mathrm{lvf}}\, e^{\lambda_{\mathrm{lvf}} V_{\mathrm{lv}}} + (1 - \mathrm{dri}\,R) \cdot P_{0\mathrm{rvf}} \cdot a_{\mathrm{rvf}}\, e^{\lambda_{\mathrm{rvf}} V_{\mathrm{rv}}}) \quad (21)$$

where a_{spt}, a_{lvf}, a_{rvf}, b_{spt}, b_{lvf}, b_{rvf} are defined:

$$x_1 = V_{\mathrm{spt,old}} + \Delta V_{\mathrm{spt}}; \quad x_2 = V_{\mathrm{spt,old}} - \Delta V_{\mathrm{spt}} \quad (22)$$

$$a_{\mathrm{spt}} = \frac{e^{\lambda_{\mathrm{spt}} x_2} - e^{\lambda_{\mathrm{spt}} x_1}}{x_2 - x_1}; \quad a_{\mathrm{lvf}} = \frac{e^{\lambda_{\mathrm{lvf}} x_2} - e^{\lambda_{\mathrm{lvf}} x_1}}{x_2 - x_1}; \quad a_{\mathrm{rvf}} = \frac{e^{\lambda_{\mathrm{rvf}} x_2} - e^{\lambda_{\mathrm{rvf}} x_1}}{x_2 - x_1} \quad (23)$$

$$b_{\mathrm{spt}} = e^{\lambda_{\mathrm{spt}} x_1} - \left(e^{\lambda_{\mathrm{spt}} x_2} - \frac{e^{\lambda_{\mathrm{spt}} x_1}}{x_2 - x_1} x_1\right) \quad (24)$$

$$b_{\mathrm{lvf}} = e^{\lambda_{\mathrm{lvf}} x_1} - \left(e^{\lambda_{\mathrm{lvf}} x_2} - \frac{e^{\lambda_{\mathrm{lvf}} x_1}}{x_2 - x_1} x_1\right) \quad (25)$$

$$b_{\mathrm{rvf}} = e^{\lambda_{\mathrm{rvf}} x_1} - \left(e^{\lambda_{\mathrm{rvf}} x_2} - \frac{e^{\lambda_{\mathrm{rvf}} x_1}}{x_2 - x_1} x_1\right) \quad (26)$$

and $V_{\mathrm{spt,old}}$ is the V_{spt} in the previous time step and $\Delta V_{\mathrm{spt}} = 0.1$ ml. Note that for the case of simulations of human $\mathrm{dri}\,L = \mathrm{dri}\,R = \mathrm{dri}\,S$.

2.1.3. *Reflex actions (human simulations)*

The effect of CVS diseases on the cardiovascular system can be significantly altered by the compensation from nervous system reflex mechanisms. Thus, reflex actions are included in the CVS model for the pulmonary embolism simulation. It is assumed that vasoconstriction is proportional to a drop in pulmonary artery pressure (P_{ao}) and is modelled by increasing the systemic vascular resistance (R_{sys}) by 34% for a drop in average P_{ao} from 100 to 80 mmHg. Other reflex mechanisms include venous constriction, increased heart rate (HR) and increased ventricular contractility [1,20]. Their activation is also assumed to be proportional to the drop in the average pressure in the aorta (P_{ao}). The proportionality constants are estimated based on clinically observed CVS hemodynamic responses reported in the literature [24–26]. More specifically, HR and ventricular contractility are increased by 80–120 beats per minute and 67% whereas the venous dead space V_{dvc} is decreased by 35% respectively for a drop in average P_{ao} to 80 mmHg. Fig. 3 shows how R_{sys} is varied as a function of ΔP_{ao}.

2.2. *Integral-based parameter identification*

To uniquely determine the parameters, the model equations are transformed using integrals. A previously designed integral-based parameter identification method [17] is extended in this paper to rapidly identify the patient-specific parameters from limited discrete data. The assumed

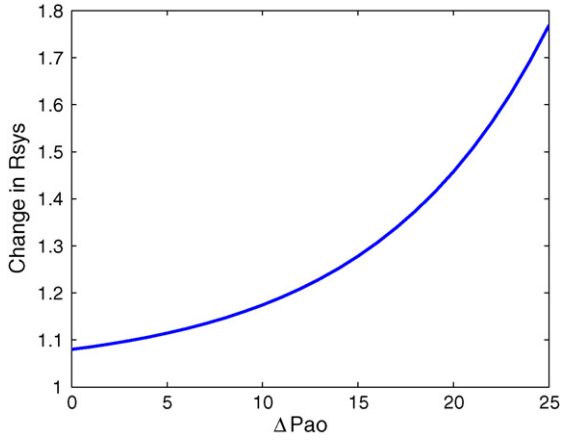

Fig. 3 – Reflex action: varying R_{sys} as a function of ΔP_{ao}.

measured data is the discrete minimum and maximum values of the pressure in the aorta ($P_{\mathrm{ao,max}}$, $P_{\mathrm{ao,min}}$), pulmonary artery ($P_{\mathrm{pa,max}}$, $P_{\mathrm{pa,min}}$), and the discrete maximum and minimum volumes of the left and right ventricles ($V_{\mathrm{lv,max}}$, $V_{\mathrm{lv,min}}$, $V_{\mathrm{rv,max}}$, $V_{\mathrm{rv,min}}$). Hence, unlike prior work [17], no waveforms are required and there are 60% less measurements (four total) required in this approach. The identified parameters, and the parameters which are either measured or taken from the literature are given in Table 2.

2.2.1. *Scaling model outputs—discrete data*

For discrete data, the waveforms are not known, therefore the integral method of [17] cannot be directly applied. However, waveforms can be artificially generated by scaling a set of previously calculated model outputs to best fit the maximum and minimum measured data values for the pressures and volumes. The estimated signals between the discrete data points are thus forced to have similar dynamics to the model, hence minimizing modelling error. In return, significantly less measurement and potentially fewer invasive catheters are required.

The scaled signal, $\mathrm{Sig}_{\mathrm{new}}$, is obtained from a previously calculated signal, $\mathrm{Sig}_{\mathrm{old}}$, as follows:

$$\mathrm{Sig}_{\mathrm{new}} = a \cdot \mathrm{Sig}_{\mathrm{old}} + b \quad (27)$$

$$a = \frac{(\mathrm{Sig}_{\mathrm{m,max}} - \mathrm{Sig}_{\mathrm{m,min}})}{(\mathrm{Sig}_{\mathrm{s,max}} - \mathrm{Sig}_{\mathrm{s,min}})} \quad (28)$$

$$b = \frac{(\mathrm{Sig}_{\mathrm{s,max}} \cdot \mathrm{Sig}_{\mathrm{m,min}} - \mathrm{Sig}_{\mathrm{m,max}} \cdot \mathrm{Sig}_{\mathrm{s,min}})}{(\mathrm{Sig}_{\mathrm{s,max}} - \mathrm{Sig}_{\mathrm{s,min}})} \quad (29)$$

where the subscript 's' refers to simulated output and the subscript 'm' refers to measured data. For example, Fig. 4 shows the pressure in the aorta (P_{ao}) after scaling with $a = 0.6832$ and

Table 2 – Parameters used in CVS model

Parameters from literature or measured: P_{th}, period, λ_{lvf}, λ_{rvf}, λ_{pcd}, $P_{0\mathrm{pcd}}$, $E_{es,spt}$, $V_{d,spt}$, $V_{0\mathrm{spt}}$, $P_{0\mathrm{spt}}$
Optimized parameters: L_{av}, L_{mt}, L_{tc}, L_{pv}, $E_{es,lvf}$, $P_{0\mathrm{lvf}}$, $E_{es,rvf}$, $P_{0\mathrm{rvf}}$, $V_{0\mathrm{pcd}}$, R_{av}, R_{mt}, R_{tc}, R_{pv}, P_{ao0}, P_{pu0}, P_{pa0}, P_{vc0}, E_{ao}, E_{pa}, E_{vc}, E_{pu}, R_{sys}, R_{pul}

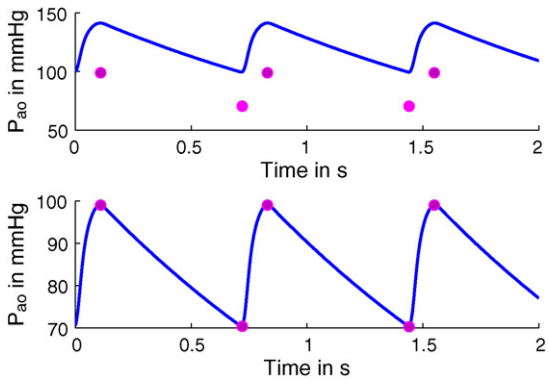

Fig. 4 – Simulated pulmonary embolism in human: pressure in aorta (P_{ao}) before and after scaling with $a = 0.6832$ and $b = 2.417$, with the measured maximum and minimum values denoted by a circle.

$b = 2.417$, with the measured maximum and minimum values denoted by a circle.

2.2.2. *Scaling model outputs—porcine data*

For the porcine data continuous waveforms are measured in V_{lv}, V_{rv}, P_{ao} and P_{pa}. However, the same scaling approach can be used to simplify the parameter identification. In particular, scaling effectively filters noise and unmodelled dynamics from the data. The identification problem is thus restricted to dynamics in the model. Note that the final comparison is still made to the original data and this approach is only done to minimize computational effort and complexity in the identification process. An example of scaling in this clinical porcine case is shown in Fig. 5, for the pressure in the aorta (P_{ao}) before and after scaling, with $a = 0.5871$ and $b = 6.7166$.

However, matching only the maximum and minimum values has the limitation that the waveform shape may not be precisely captured. For the porcine data, better matches to the waveform shapes were obtained by introducing a slight nonlinearity into the pressure volume relationship in the aorta and pulmonary artery, as defined by Eq. (10). A range of f parameters ranging from 0.8 to 1.4 were tested, where each time the integral method was applied. The f value producing the best waveform match in the aorta and pulmonary artery was chosen. Hence, more complexity could be readily added to the model to better capture the observed dynamics with minimal effect on computational time.

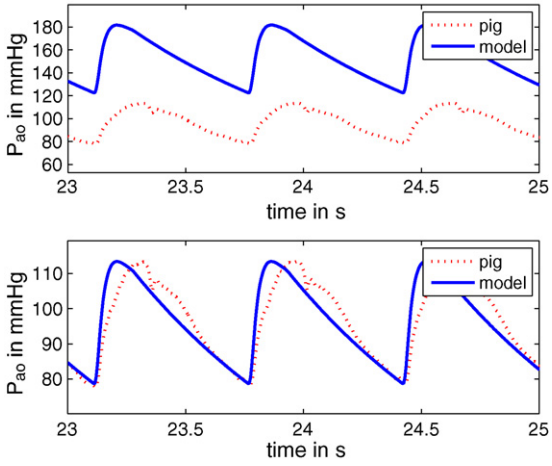

Fig. 5 – Porcine pulmonary embolism: pressure in aorta (P_{ao}) before and after scaling with $a = 0.5871$ and $b = 6.7166$. The dotted line represents the measured, clinical porcine data. The solid line represents the model data before (upper panel) and after (lower panel) scaling.

2.2.3. *Integral identification problem formulation*

Consider the left ventricle defined in Eqs. (8) and (13). Assume that Q_{av}, Q_{mt}, P_{ao}, V_{lv}, V_{spt} and P_{peri} are either measured or estimated from measured data. Integrating Eq. (11) from t_{eb} to t during ejection and from t_{fb} to t during filling gives an expression for $V_{lv}(t)$ [17]:

$$V_{lv}(t) = V_{lv}(t_{eb}) - \int_{t_{eb}}^{t} Q_{av}(t)\,dt, \quad t_{eb} \le t \le t_{ef} \tag{30}$$

$$V_{lv}(t) = V_{lv}(t_{fb}) + \int_{t_{fb}}^{t} Q_{mt}(t)\,dt, \quad t_{fb} \le t \le t_{fe} \tag{31}$$

where t_{eb} is the beginning of ejection, and t_{fb} is the beginning of filling, t_{ee} stands for end-ejection and t_{fe} for end-filling respectively. For simplicity, $V_{dao} = 0$ and $f = 1$ in the following equations.

Integrating Eq. (8) from 0 to t, solving for $V_{ao}(t)$, and then using Eqs. (9) and (10) yields:

$$P_{ao}(t) = E_{ao}\left(V_{ao}(0) + \int_0^t Q_{av}(t)\,dt - \frac{1}{R_{sys}}\int_0^t P_{ao}(t)\,dt - \frac{1}{R_{sys}}\int_0^t P_{vc}(t)\,dt\right) \tag{32}$$

Under the assumption that $P_{vc} = P_{vc0}$ is an unknown constant, Eq. (32) can be rewritten:

$$P_{ao}(t) = P_{ao0} + E_{ao}\int_0^t Q_{av}(t)\,dt + A_1\int_0^t P_{ao}(t)\,dt + A_2 t \tag{33}$$

where A_1 and A_2 are defined:

$$A_1 = -\frac{E_{ao}}{R_{sys}}, \quad A_2 = \frac{E_{ao}P_{vc0}}{R_{sys}} \tag{34}$$

The best linear least squares fit of Eq. (34) to the measured pressure waveform P_{ao} over one heart beat will determine E_{ao} and R_{sys} over that heart beat. Similarly, given an approximation to V_{spt} and P_{peri} in Eqs. (5), (12) and (13) can be integrated across the filling and ejection stages respectively. A linear least-squares optimization can then be similarly used to determine R_{av}, R_{mt}, E_{eslvf} and P_{0lvf}. The right ventricle can be treated similarly.

Given the pressure waveforms through the aorta and pulmonary artery, the flows into and out of the left and right ventricles, as well as their volumes, a system of linear equations can thus be defined for the full CVS model [17]:

$$A \cdot \vec{x} = \vec{b} \tag{35}$$

$$\vec{x} = (L_{av}, L_{mt}, L_{tc}, L_{pv}, E_{eslvf}, P_{0lvf}, E_{esrvf}, P_{0rvf}, V_{0pcd}, E_{ao}, E_{pa}, E_{vc}, E_{pu}, R_{av}, R_{mt}, R_{tc}, R_{pv}, P_{ao0}, P_{pu0}, P_{pa0}, P_{vc0}, R_{sys}, R_{pul})^T \quad (36)$$

with $\vec{x}$ being the solution vector of the parameters to be identified, which can be found by linear least squares. More details about this integral method and parameter definitions can be found in [17,18].

Ventricular interaction is also included, however the volume of the septum is not known and not directly measurable in an ICU. As an initial approximation, this volume is set to zero. The resulting parameters identified by the integral method are then used to resimulate the model and produce an approximation of the septum volume (V_{spt}). The parameter identification is then run a second time using this V_{spt} value, producing a modified set of identified parameters that better account for ventricular interaction.

In this research, the parameters are identified for each period of measured data during the porcine experiment of pulmonary embolism. Thus, time varying changes from the initial healthy state to the fully diseased state are captured, as might be desired for a clinical system. Hence, model identification can provide a potential means of monitoring CVS disease state in the highly dynamic critical care patient.

2.2.4. *Simulation using optimized parameters*

Fig. 6 shows the overall process of the simulation and parameter identification algorithm. After the porcine-specific parameters have been identified for a respective point in time, these parameters are then used to rerun the model simulation. The simulated output is then compared to the clinical data. However, due to errors in the initial approximations of V_{spt} and the unmeasured flows (Q_{av}, Q_{mt}, Q_{pv}, Q_{tc}), and the process of scaling output signals, parameter identification should be iterated to ensure optimal convergence. Fast convergence consistently occurred within 3–5 iterations in this study and is stopped when the relative error between model output and clinical data reaches a set tolerance.

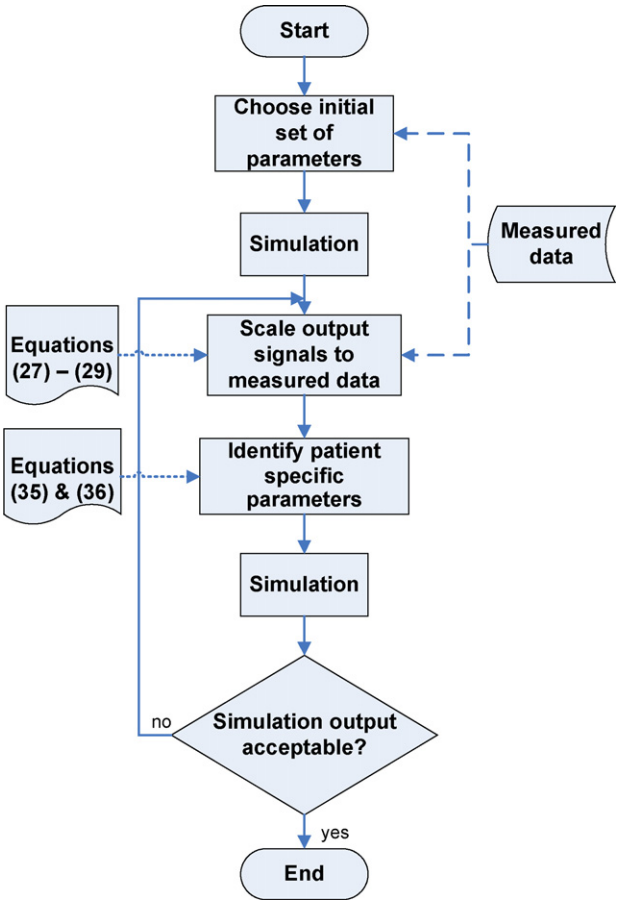

Fig. 6 – Flow chart of simulation and parameter identification algorithm. As first step, a set of parameters is used for an initial simulation, the data is then scaled to match the measured data and identified. This process is repeated until the simulation output is acceptable.

3. Results and discussion

3.1. *Simulated pulmonary embolism in human*

The CVS model and previously identified human parameters [17,12–14] are used to generate simulated pulmonary embolism data. Pulmonary embolism is caused by a blood clot obstructing the pulmonary circulation and is simulated by increasing the pulmonary resistance R_{pul} by 30% every 50 heart beats for a total of 300 heart beats. This gives an overall increase in R_{pul} of 150%. To account for measurement noise, white Gaussian noise of 5% and 10% is added to the (simulated) measurements for pressure in the aorta, pulmonary artery and both ventricle volumes.

During pulmonary embolism, blood is backing up in the right ventricle due to increased afterload. The overfilled right ventricle compresses the underfilled left ventricle and thus, the right ventricle expansion index (RVEDV/LVEDV) increases [27,28]. Fig. 7 shows the true expansion index versus the re-simulated expansion indexes obtained using the identified parameter sets from the simulated pulmonary embolism experiment.

The left panels of Fig. 8 show the simulated pressure in the left ventricle (P_{lv}), the left ventricle volume (V_{lv}) and the pressure in the aorta (P_{ao}). In each case, 10% Gaussian white noise is added to the pressure and volume signals, except for the ventricular pressure (top panel) as it is not measured or used in the analysis. Only the maximum and minimum values of P_{ao} and V_{lv} in the noise corrupted signals are used to identify the system parameters. The dotted lines in each panel are the re-simulated signals generated with the identified parameter set. Similar results for the right ventricle are given in the right panel. Although the pressure in left and right ventricles is not known and not used during the parameter identification process, the re-simulated data matches it very well.

Finally, Fig. 9 shows the identified pulmonary resistance over the 300 heart beats. Increased pulmonary resistance is the hallmark of pulmonary embolism. Here, it is consistently detected with up to 10% random noise added.

The pressure–volume relationship for the left ventricle is shown in Fig. 10 for 6 different points in time during the

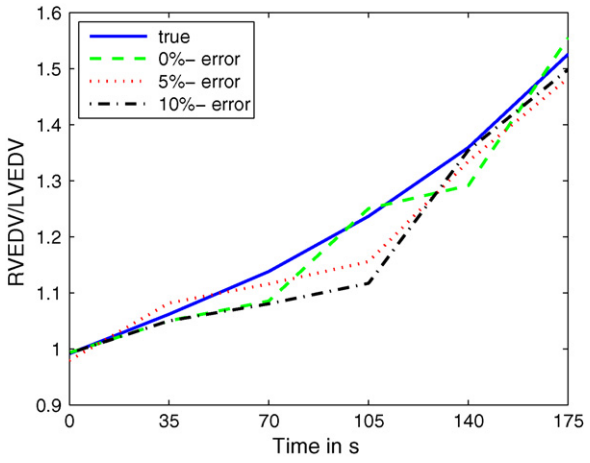

Fig. 7 – Right ventricle expansion index, RVEDV/LVEDV for 0%, 5% and 10% measurement noise added for simulated human case. The true expansion index (solid line) is shown versus the re-simulated expansion indexes (dashed and dotted lines) as obtained using the identified parameter sets from the simulated human pulmonary embolism experiment.

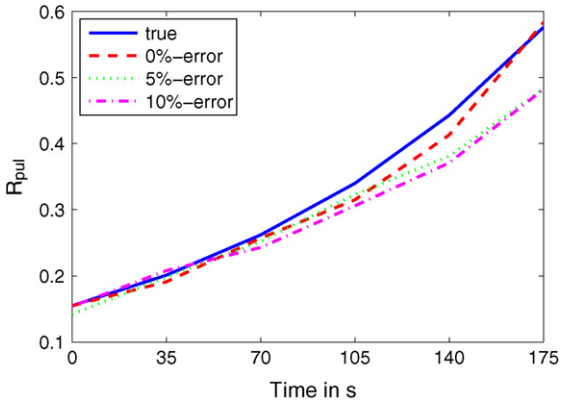

Fig. 9 – Identified pulmonary vascular resistance (R_{pul}) for 0%, 5% and 10% measurement noise added for simulated human case. The solid line represents the true resistance and the dashed and dotted line the identified resistances.

pulmonary embolism experiment with 10% measurement noise. The CVS identification method produces parameters, which when re-simulated match the clinical data very closely with average errors of 3.18 ± 1.79 mmHg (7.20%) and 3.81 ± 3.38 ml (4.67%) for the maximum and minimum pressures and volumes respectively. These identification results are summarized in Table 3, which also shows an accurately captured rise in pulmonary resistance.

3.2. *Integral versus derivative identification approaches*

Rather than formulating Eqs. (1)–(13) in terms of integrals [17] a potentially simpler way is to directly substitute the measured or estimated data into Eqs. (1)–(13). This approach would require differentiating the signals for Eqs. (8), (11), (12) and (13). For the case of scaled signals, the local noise is effectively removed and the signals are smooth suggesting that differentiation may be suitable. A similar system of linear equations to Eqs. (35) and (36) would be obtained without the initial conditions P_{ao0}, P_{pa0}, P_{vc0} and P_{pu0} which are essentially integration constants.

However, although local measurement noise is removed there is still modelling error that occurs from scaling the signals. Specifically, a scaled waveform can only match the maximum and minimum values of a measured signal and will not necessarily have the same waveform shape. Fig. 11 shows an example where the scaled and measured pressure and volume waveforms are superimposed. Note that "measured" in this case refers to the model generated signal using pre-selected parameters that represent a "virtual" patient.

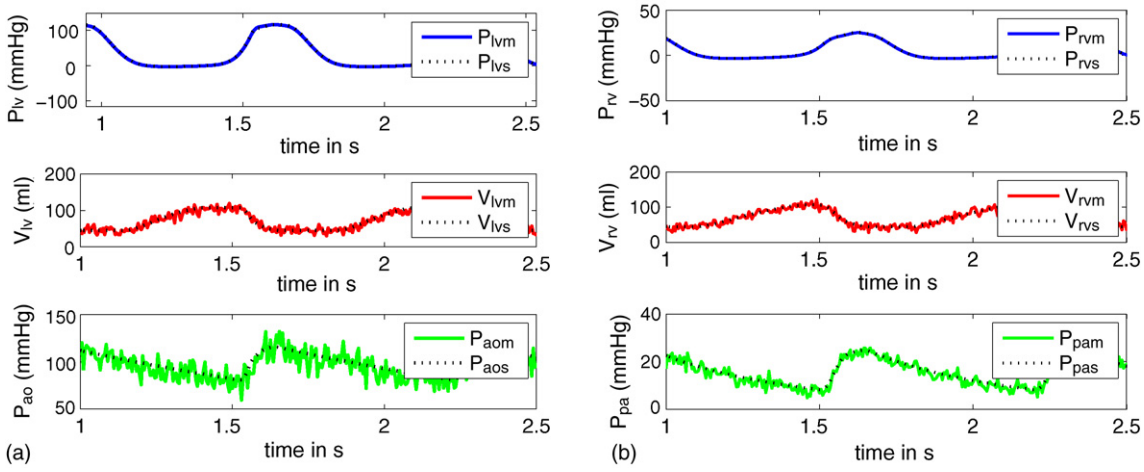

Fig. 8 – Integral-based identification (ID): pressures and volumes, measured (m) vs. simulated (s) for simulated human case. The upper panels shows the pressures in left/right ventricles (P_{lv}, P_{rv}), the middle panels show the volumes in left/right ventricles (V_{lv}, V_{rv}) and the lower panels show the pressure in aorta (P_{ao}) and pulmonary artery (P_{pa}), respectively: (a) left ventricle; (b) right ventricle.

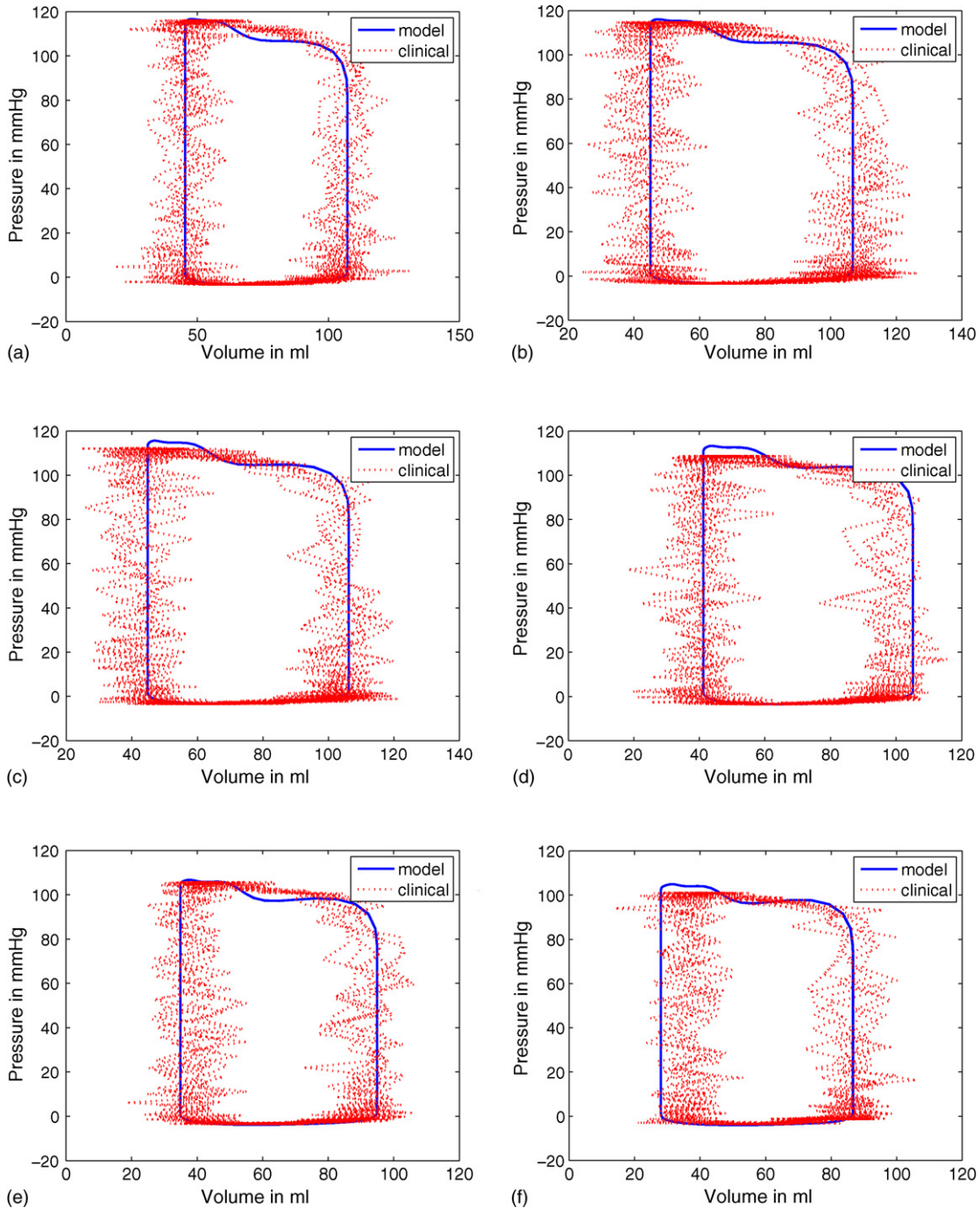

Fig. 10 – Pressure–volume relationship for left ventricle during different stages of the simulated human pulmonary embolism experiment with 10% measurement noise added. The solid lines represent model output and the dotted lines measured data: (a) time: 0 s; (b) time: 35 s; (c) time: 70 s; (d) time: 105 s; (e) time: 140 s; (f) time: 175 s.

Fig. 12 shows a comparison of the derivatives dP_{ao}/dt, dP_{pa}/dt and integrals $\int_0^t P_{ao}\,dt$, $\int_0^t P_{pa}\,dt$ for the scaled versus true signals. A similar comparison is made between dV_{lv}/dt, dV_{rv}/dt and $\int_0^t V_{lv}\,dt$, $\int_0^t V_{rv}\,dt$ in Fig. 13. Very large errors can be seen in the differentiated signals, thus showing how differentiation amplifies the modelling error between the curves in Fig. 11, even though the signals are locally smooth. In contrast, integration effectively reduces modelling error as shown by the upper panels in Figs. 12 and 13. Figs. 14 and 15 further demonstrate the differences by displaying the percentage errors for both methods, where the derivative-based approach shows an effective instability.

The parameters identified by the derivative-based method are then used to rerun the CVS model and produce pressure and volume curves, for comparison to the measured (simulated) data. This process is repeated in all the measured periods during the pulmonary embolism simulation experiment. The results in Fig. 16 show significantly large errors

Table 3 – Simulated human pulmonary embolism: mean model response errors and standard deviation for combined maximum and minimum pressures and volumes

Noise (%)	P_{ao}	P_{pa}	P_{lv}	P_{rv}
Pressures (mmHg) and error (%)				
0	1.63 ± 0.89 (1.70)	1.28 ± 1.31 (4.92)	1.30 ± 1.56 (2.40)	0.76 ± 1.38 (4.17)
5	1.58 ± 0.83 (1.74)	2.01 ± 1.60 (7.74)	0.69 ± 0.75 (4.40)	1.39 ± 1.56 (9.01)
10	3.18 ± 1.79 (3.57)	2.72 ± 1.96 (9.33)	1.36 ± 1.63 (6.29)	1.76 ± 1.99 (9.62)

Noise (%)	V_{rv}	V_{lv}
Volumes (ml) and error (%)		
0	1.72 ± 1.36 (2.46)	1.80 ± 2.08 (2.46)
5	2.07 ± 1.08 (3.36)	2.88 ± 2.34 (3.81)
10	2.50 ± 2.44 (4.64)	3.81 ± 3.38 (4.70)

Noise (%)	0 s	35 s	70 s	105 s	140 s	175 s
R_{pul} (mmHg s ml^{-1}) and error (%)						
0	0.15 (0.07)	0.19 (5.34)	0.25 (1.72)	0.31 (7.32)	0.41 (6.62)	0.58 (1.32)
5	0.14 (8.06)	0.19 (1.40)	0.25 (3.81)	0.32 (5.06)	0.38 (14.04)	0.48 (16.16)
10	0.15 (0.14)	0.20 (2.10)	0.24 (7.34)	0.30 (10.01)	0.37 (16.14)	0.48 (16.23)
True	0.15	0.20	0.26	0.34	0.44	0.57

The lower portion shows the value of pulmonary resistance, R_{pul}, with the true simulated value for comparison. The mean percentage errors are given in parenthesis.

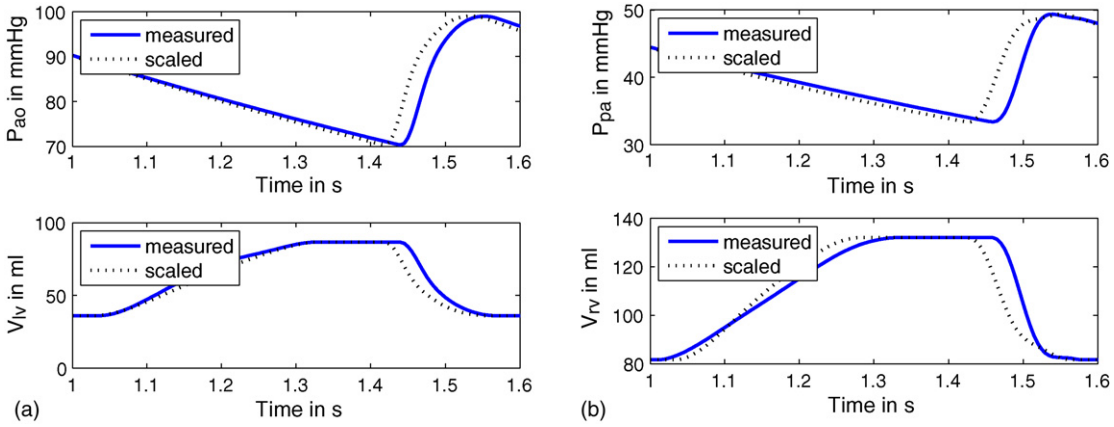

Fig. 11 – Comparison between measured (solid) and scaled (dashed) signals for simulated human case: (a) left ventricle; (b) right ventricle.

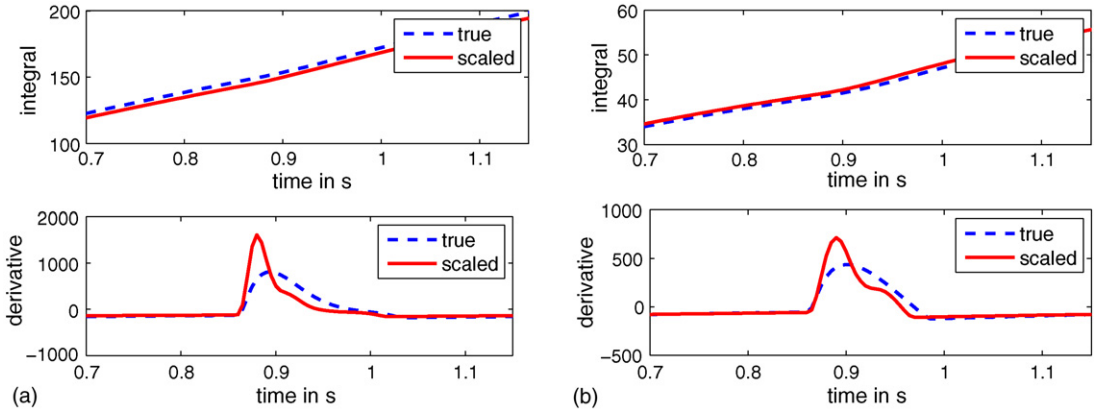

Fig. 12 – Comparison between integral and derivative for true (dashed) and scaled (solid) signal for simulated human case. The very large errors in the differentiated signals show how differentiation amplifies the modelling error: (a) pressure in aorta, P_{ao}; (b) pressure in pulmonary artery, P_{pa}.

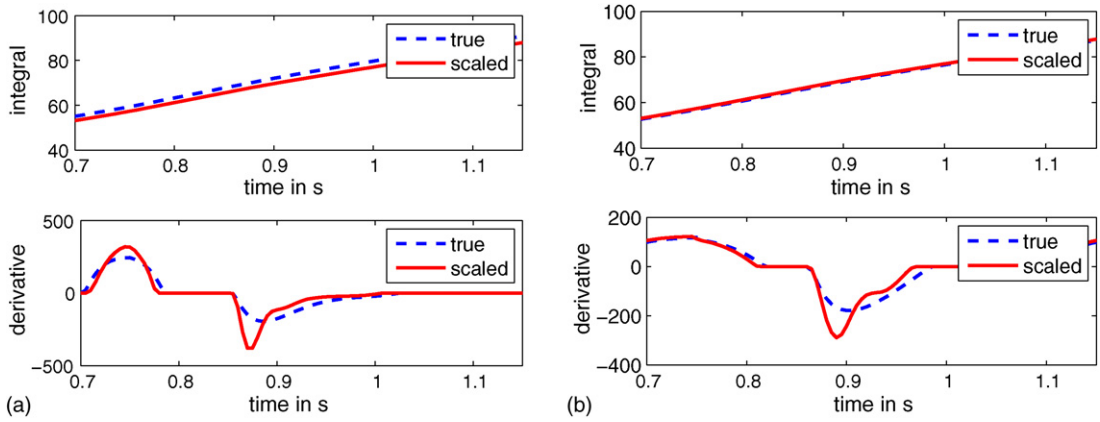

Fig. 13 – Comparison between integral and derivative for true (dashed) and scaled (solid) signal for simulated human case. The very large errors in the differentiated signals show how differentiation amplifies the modelling error: (a) volume in left ventricle, V_{lv}; (b) volume in right ventricle, V_{rv}.

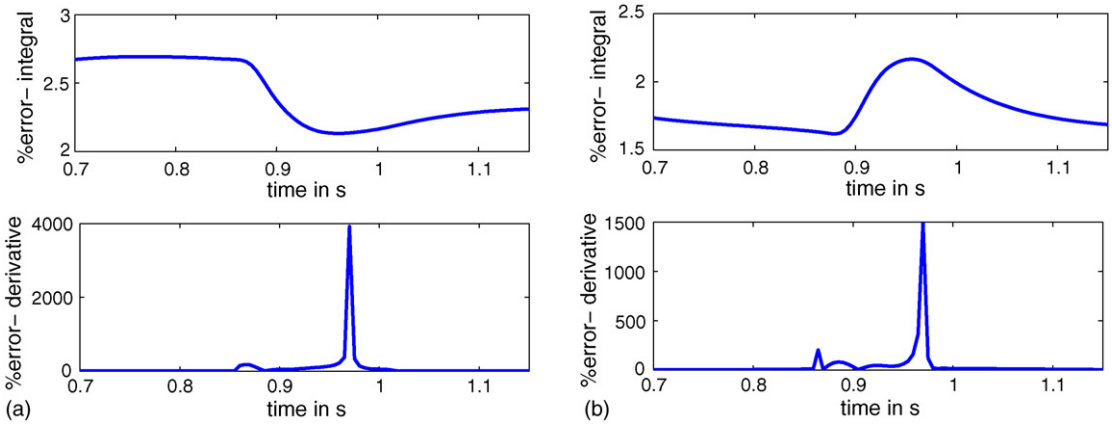

Fig. 14 – Percentage error for integral and derivative for simulated human case: (a) pressure in aorta, P_{ao}; (b) pressure in pulmonary artery, P_{pa}.

in the matching of the signals. The total mean error in the identified parameters, versus the true values simulated, over all periods for the derivative-based method was 419 ± 1363%, with noise at 10%. In comparison, the total mean error in the identified parameters for the integral-based approach applied on the same data set, was 9 ± 16%. Thus, the integral formulation provides a robust parameter identification in the presence of modelling as well as measurement error.

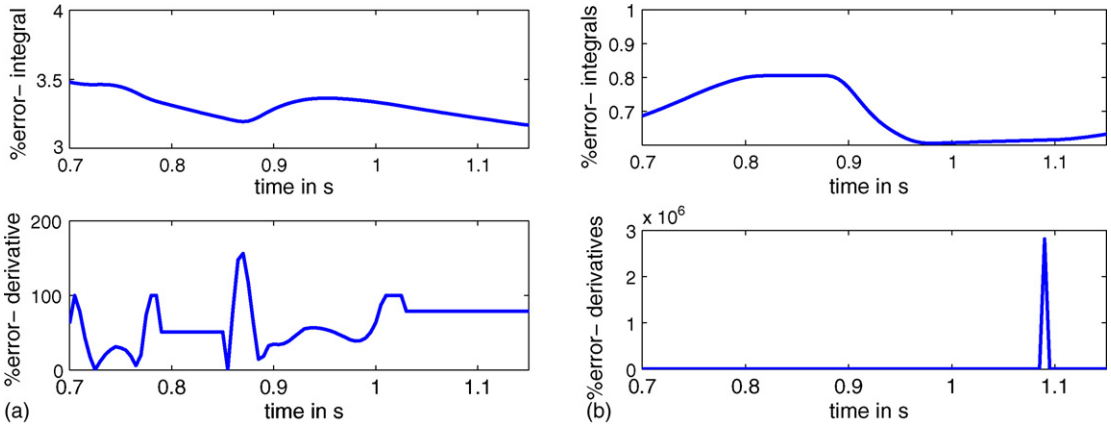

Fig. 15 – Percentage error for integral and derivative for simulated human case: (a) volume in left ventricle, V_{lv}; (b) volume in right ventricle, V_{rv}.

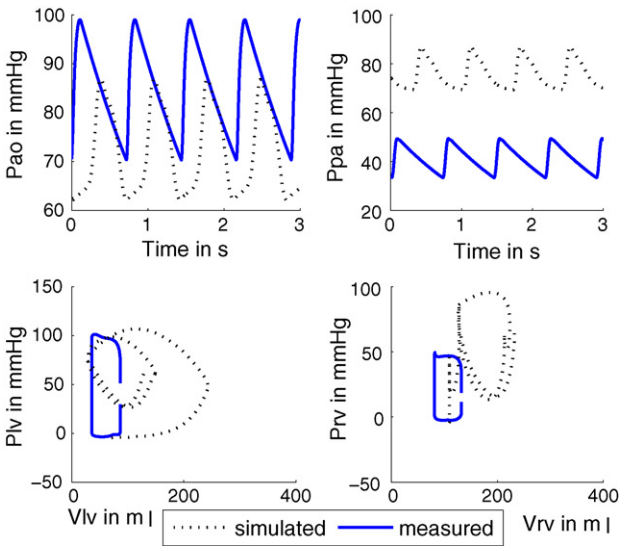

Fig. 16 – Derivative-based identification (ID): pressures and volumes, measured vs. simulated, for a simulated human trial of pulmonary embolism. The upper panels show the true (solid) vs. re-simulated (dotted) pressure in aorta (P_{ao}) and pulmonary artery (P_{pa}). The lower panels show the true (solid) vs. re-simulated (dotted) pressure–volume relationships for the left and right ventricles.

3.3. *Porcine pulmonary embolism*

Finally, the integral-based parameter identification is applied to clinical porcine data for a true clinical validation. The data was obtained from the Hemodynamics Research Laboratory, University of Liège, Belgium. In the experiments, a pig is injected with autologous blood clots every 2 h to simulate pulmonary embolism [29]. Three pigs are presented for initial validation of the methods presented.

Fig. 17 shows the simulated model output for the pressure in the left and right ventricles (P_{lvs}, P_{rvs}), the volume in the left and right ventricles (V_{lvs}, V_{rvs}) and the pressure in the aorta, pulmonary artery (P_{aos}, P_{pas}) overlaid with the corresponding clinical data (P_{lvp}/P_{rvp}, V_{lvp}/V_{rvp}, P_{aop}/P_{pap}) at 30 min into the pulmonary embolism experiment of pig 1. The simulation data matches the measured porcine data very well with errors within 2.36 mmHg (~ 5.72%) and 1.47 ml (~ 2.16%) for the maximum and minimum pressures and volumes, respectively.

Fig. 18 shows the volume–pressure waveforms for the left and right ventricles in more detail. The upper panel in Fig. 18 is the simulated ventricle volume and the dotted line is the measured porcine volume for two heartbeats. The lower panel shows the same results obtained for the ventricle pressure. Finally, Fig. 19 shows the resulting pressure–volume relationships (*P–V* loops) for the left and right ventricles. Errors in all cases are in the range of 0.15–4.76%.

Fig. 20 displays the *P–V* loops for the left and right ventricle 120 min into the pulmonary embolism experiment. Although the model did not exactly capture all the exact volume shapes in the left and right ventricles, the pressure waveform shapes were accurately captured, as well as the maximum and minimum pressures and volumes. The differences represent local, unmodelled dynamics, as might be expected. Overall, the errors in the maximum pressures and volumes that are typically used to define trends in different disease states are within 0.17–4.95%, respectively.

Fig. 21 displays the *P–V* loops at 180 min, which was the end of the experiment. Again the results show a very close match. Errors in the maximum pressures and volumes are all within 0.20% and 6.59%, respectively.

Fig. 22 clearly shows that the identified subject (pig) specific parameters systemic and pulmonary vascular resistance, R_{sys} and R_{pul}, differ significantly between healthy and disease state, with R_{pul} increasing by 261.44%. Furthermore, the model's ability to pick up reflex response can clearly be seen in Fig. 22, as the pig increases systemic resistance to help restore

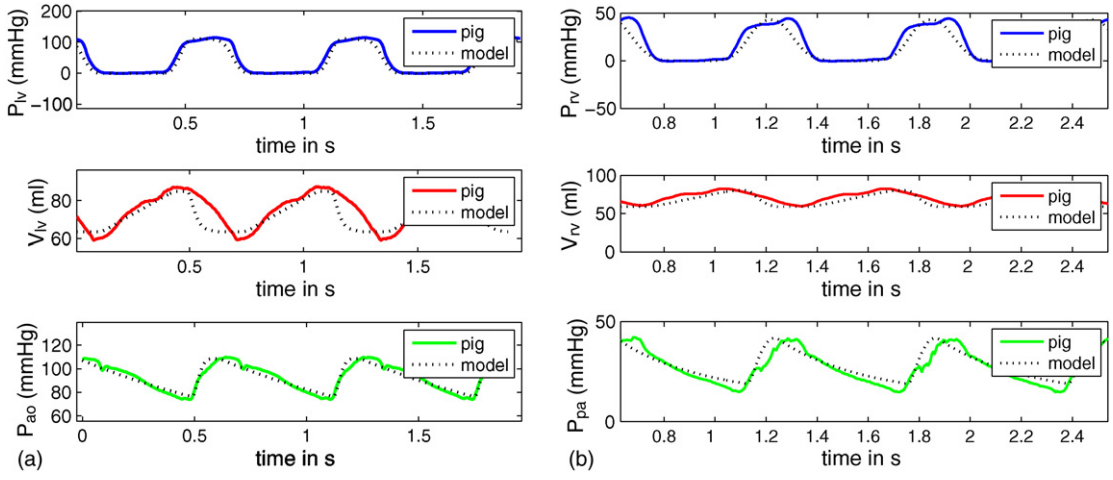

Fig. 17 – Porcine pulmonary embolism, pig 1, model output (dotted) vs. clinical (solid) data. The upper panels show the pressure in left/right ventricle (P_{lv}, P_{rv}). The middle panels show the volumes in left/right ventricle (V_{lv}, V_{rv}) and the lower panels show the pressure in aorta and pulmonary artery (P_{ao}, P_{pa}): (a) 30 min, left ventricle; (b) 30 min, right ventricle.

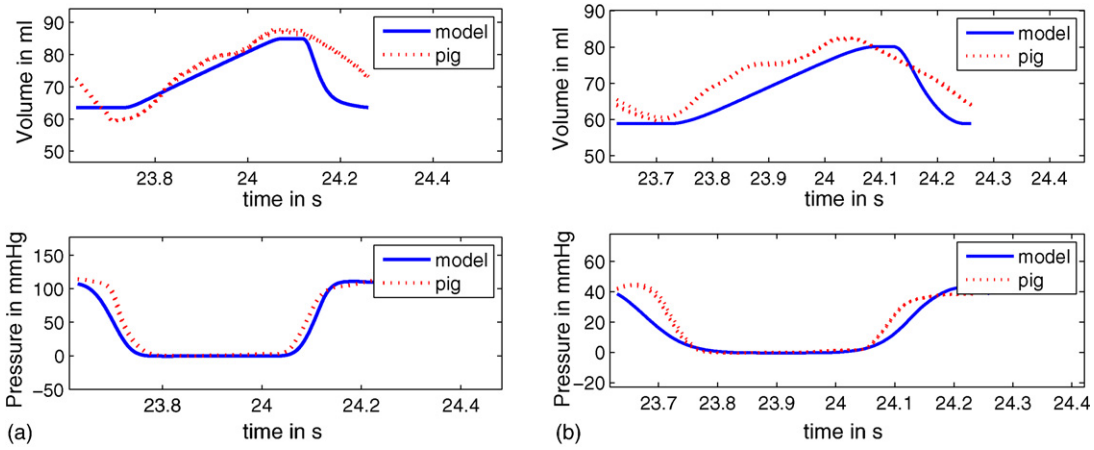

Fig. 18 – Porcine pulmonary embolism, pig 1, model output (solid) vs. clinical (dotted) data for pressure and volume. The upper panels show the volumes and the lower panels the pressures in the left and right ventricles: (a) 30 min, left ventricle; (b) 30 min, right ventricle.

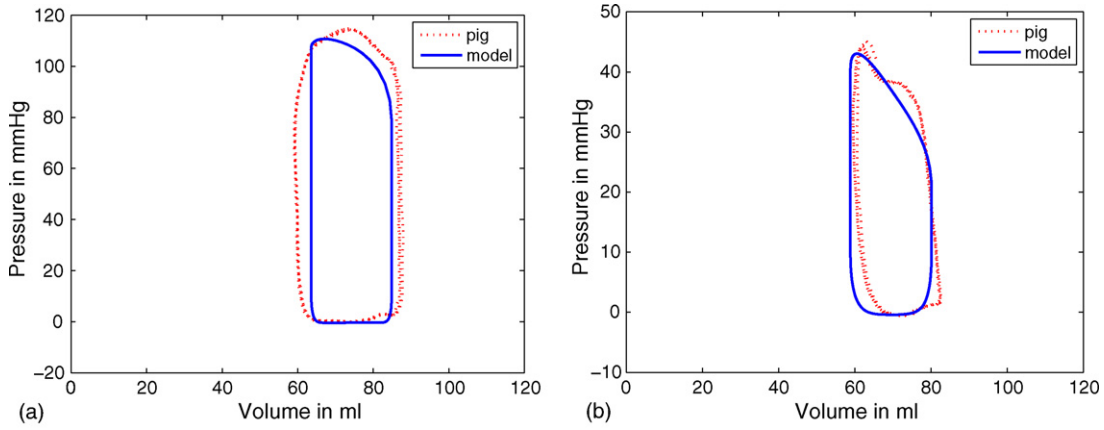

Fig. 19 – Porcine pulmonary embolism, pig 1, pressure–volume relationship for left and right ventricle as obtained when re-simulated using the CVS model and identified pig-specific parameters: (a) 30 min, left ventricle; (b) 30 min, right ventricle.

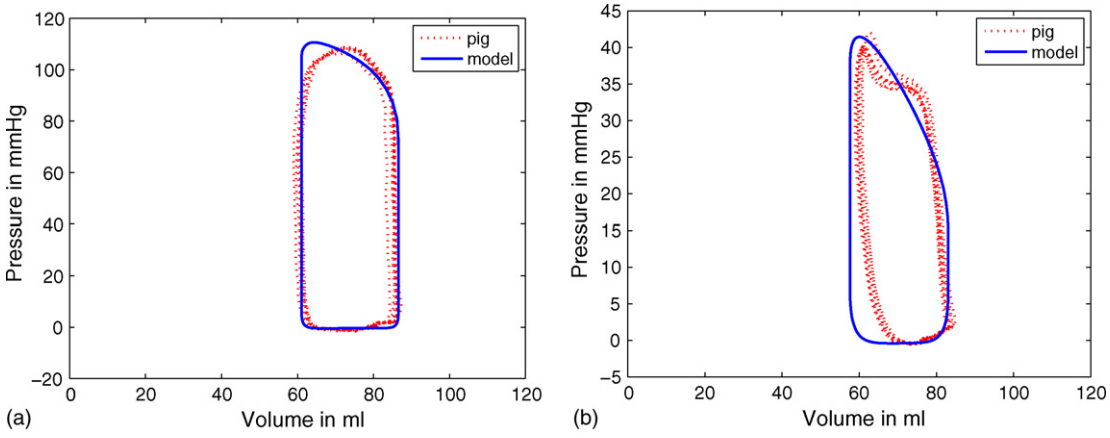

Fig. 20 – Porcine pulmonary embolism, pig 1, pressure–volume relationship for left and right ventricle as obtained when re-simulated using the CVS model and identified pig-specific parameters: (a) 120 min, left ventricle; (b) 120 min, right ventricle.

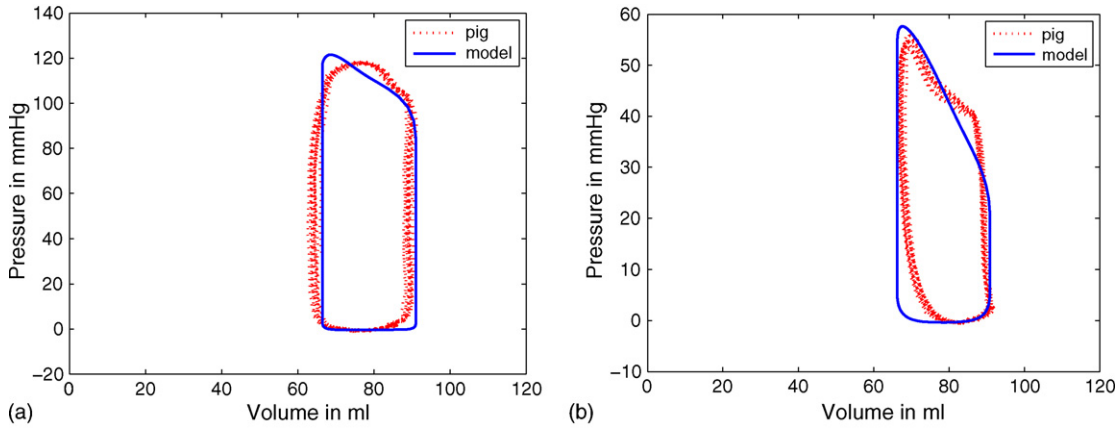

Fig. 21 – Porcine pulmonary embolism, pig 1, pressure–volume relationship for left and right ventricle as obtained when re-simulated using the CVS model and identified pig-specific parameters: (a) 180 min, left ventricle; (b) 180 min, right ventricle.

blood pressure. However, near the end, when the pig is near death, systemic resistance (R_{sys}) drops off. This last result is potentially a sign that the pig can no longer regulate hemodynamics effectively. The left and right ventricle contractilities (E_{eslvf}, E_{esrvf}) also increased during the pulmonary embolization experiment. These contractilities are also known to be part of reflex response [30], providing some further confirmation of this result.

The derivative formulation of the parameter identification algorithm did not produce a parameter set that could be used to re-run the CVS simulation when using the clinical porcine data. This result further illustrates the instability and/or difficulty of this type of method for this problem.

3.4. *Summary of three pigs*

The results of the integral-based parameter identification method on the three pigs are summarized in Table 4. The mean and standard deviation of the absolute errors for the maximum and minimum pressure in aorta (P_{ao}) and pulmonary artery (P_{pa}), and left and right ventricle (P_{lv}, P_{rv}) are given. The mean model response errors are within 2.21 ± 2.15 mmHg ($\sim 5.52\%$) for the pressures and 2.37 ± 2.01 ml ($\sim 3.49\%$) for the volumes. These results show that the minimal CVS model is able to capture the essential dynamics of the porcine CVS response to induced pulmonary embolism, over a selection of subjects.

Table 4 – Porcine pulmonary embolism: mean model response errors and standard deviation for combined maximum and minimum pressures and volumes

Pig #	P_{ao}	P_{pa}	P_{lv}	P_{rv}
Pressures (mmHg) and volumes (ml)				
1	3.50 ± 3.24 (4.10)	2.31 ± 1.93 (8.63)	1.37 ± 1.65 (3.46)	2.31 ± 1.93 (5.46)
2	5.04 ± 3.16 (4.59)	2.39 ± 1.82 (10.17)	1.60 ± 1.17 (1.90)	1.26 ± 1.33 (5.23)
3	2.56 ± 2.13 (2.18)	2.30 ± 1.79 (2.30)	2.41 ± 2.60 (2.41)	0.57 ± 0.70 (2.51)
Noise (%)		V_{rv}		V_{lv}
Volumes (ml) and error (%)				
0		1.66 ± 1.68 (2.39)		1.27 ± 1.18 (1.90)
5		3.46 ± 0.87 (4.21)		3.00 ± 1.60 (4.75)
10		3.31 ± 2.31 (5.67)		2.29 ± 2.15 (3.32)

Pig (#)	0 min	60 min	90 min	120 min	180 min	240 min
R_{pul} (mmHg s ml^{-1})						
1	0.04	0.19	0.19	0.19	0.30	0.29
2	0.15	0.30	0.39	0.38	0.52	0.46
3	0.13	0.17	0.21	0.22	0.40	0.44

The lower portion shows the true value of pulmonary resistance, R_{pul}, with the true simulated value for comparison. The mean percentage errors are given in parenthesis.

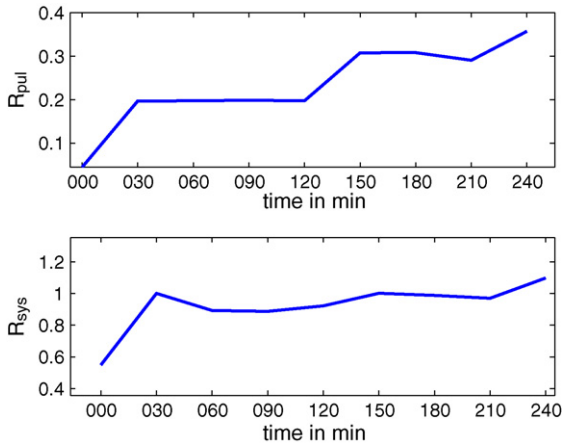

Fig. 22 – Porcine pulmonary embolism, pig 1: pulmonary (upper panel) and vascular systemic (lower panel) resistance as identified during the pulmonary embolism experiment.

4. Conclusions

The integral-based optimization successively identified patient specific parameters for the minimal cardiac model with inertial effects and ventricular interaction. A much reduced discrete set of measured data was employed compared to prior work. The use of integrals for identification of this model parameter identification, particularly in the presence of measurement noise and/or modelling error. In contrast, derivative-based methods failed to produce stable, reliable identification results. Thus, integrals are fundamental to handling both local measurement error [17] and modelling error in the parameter identification process. Computationally, the parameter identification optimization problem is made linear and convex, where current approaches are non-linear and non-convex. The results from clinical porcine data of pulmonary embolism show that clinically relevant and physiologically accurate parameter identification can be obtained to a clinical setting. These results will obviously need to be confirmed with further trials over broader sets of cardiac circulatory dysfunction. However, this integral approach has the potential to ensure medical staff can obtain rapid patient specific information to assist in diagnosis and therapy selection in clinical real-time.

REFERENCES

[1] A. Grenvik, S.M. Ayres, P.R. Holbrook, W.C. Shoemaker (Eds.), Textbook of Critical Care, 2nd ed., W.B. Saunders Company, 1989.
[2] A.C. Guyton, J.E. Hall, Textbook of Medical Physiology, 10th ed., Saunders, Philadelphia, 2000.
[3] C.S. Peskin, D.M. McQueen, Cardiac fluid dynamics, Rev. Biomed. Eng. 20 (5–6) (1992) 451–459.
[4] D.M. McQueen, C.S. Peskin, E.L. Yellin, Fluid dynamics of the mitral valve: physiological aspects of mathematical model, Am. J. Physiol. 242 (6) (1982) H1095–H1110.
[5] I.J. Legrice, P.J. Hunter, B.H. Smaill, Laminar structure of the heart: mathematical model, Am. J. Physiol. 272 (1997) H2466–H2476.
[6] P.J. Hunter, B.H. Smaill, Structure and Function of the Diastolic Heart: Material Properties of Passive Myocardium, in: L. Glass, P. Hunter, A. McCulloch (Eds.), Theory of Heart, Springer-Verlag, Harrisonburg, 1991.
[7] D.C. Chung, S.C. Niranjan, J.W. Clark, A. Bidani, W.E. Johnston, J.B. Zwischenberger, D.L. Traber Jr., A dynamic model of ventricular interaction and pericardial influence, Am. J. Physiol. 272 (6 Pt 2) (1997) H2942–H2962.
[8] M. Ursino, A mathematical model of the carotid baroregulation in pulsating conditions, IEEE Trans. Biomed. Eng. 4 (1999) 382–392.
[9] N. Stergiopulos, P. Segers, N. Westerhof, Use of pulse pressure method for estimating total arterial compliance in vivo, Am. J. Physiol. 276 (2 Pt 2) (1999) H424–H428.
[10] J.T. Ottesen, M.S. Olufsen, J.K. Larsen, Applied Mathematical Models in Human Physiology, Society for Industrial and Applied Mathematics, Philadelphia, 2004.
[11] R. Mukkamala, R.J. Cohen, A forward model-based validation of cardiovascular system identification, Am. J. Physiol. Heart Circ. Physiol. 281 (6) (2001) H2714–H2730.
[12] B.W. Smith. Minimal haemodynamic modelling of the heart & circulation for clinical application, PhD thesis, University of Canterbury, 2004.
[13] B.W. Smith, J.G. Chase, G.M. Shaw, R.I. Nokes, Experimentally verified minimal cardiovascular system model for rapid diagnostic assistance, Control Eng. Pract. 13 (2005) 1183–1193.
[14] B.W. Smith, J.G. Chase, G.M. Shaw, R.I. Nokes, Simulating transient ventricular interaction using a minimal cardiovascular system model, Physiol. Meas. 27 (2006) 165–179.
[15] B.W. Smith, J.G. Chase, R.I. Nokes, G.M. Shaw, G. Wake, Minimal haemodynamic system model including ventricular interaction and valve dynamics, Med. Eng. Phys. 26 (2004) 131–139.
[16] C.E. Hann, J.G. Chase, G.M. Shaw, Efficient implementation of non-linear valve law and ventricular interaction dynamics in the minimal cardiac model, Comput. Meth. Programs Biomed. 80 (2005) 65–74.
[17] C.E. Hann, J.G. Chase, G.M. Shaw, Integral-based identification of patient specific parameters for a minimal cardiac model, Comput. Meth. Programs Biomed. 81 (2) (2006) 181–192.
[18] C.E. Hann, S. Andreassen, B.W. Smith, G.M. Shaw, J.G. Chase, Identification of time-varying cardiac disease state using a minimal cardiac model with reflex actions, in: Proceeding of 14th IFAC Symposium on System Identification (SYSID 2006), Newcastle, Australia, March 29–31, 2006.
[19] B.W. Smith, J.G. Chase, R.I. Nokes, G.M. Shaw, G. Wake, Minimal haemodynamic system model including ventricular interaction and valve dynamics, Med. Eng. Phys. 26 (2) (2004) 131–139.
[20] R.E. Klabunde, Cardiovascular Physiology Concepts, Lippincott Williams and Wilkins, 2004.
[21] C. Ramanathan, J. Ping, R. Ghanem, K. Ryu, Y. Rudy, Activation and repolarization of the normal human heart under complete physiological conditions, Proc. Natl. Acad. Sci. Am. 103 (16) (2006) 6309–6314.
[22] K.T. Weber, J.S. Janicki, S. Shroff, A.P. Fishman, Contractile mechanics and interaction of the right and left ventricles, Am. J. Cardiol. 47 (1981) 686–695.
[23] M.A. Fogel, P.M. Weinberg, K.B. Gupta, J. Rychik, A. Hubbard, E.A. Hoffman, J. Haselgrove, Mechanics of the single left ventricle: a study in ventricular-ventricular interaction II, Circulation 98 (1998) 330–338.

[24] E. Braunwald, Heart Disease, A Text Book of Cardiovascular Medicine, 5th ed., W.B. Saunders Company, Philadelphia, 1997.
[25] A. Despopoulos, S. Silbernagl, Color Atlas of Physiology, 5th ed., Thieme, New York, 2001.
[26] J.E. Parrillo, R.C. Bone, Critical Care Medicine, Principles of Diagnosis and Management, St. Louis, Missouri, Mosby, 1995.
[27] C.T. Gan, J.W. Lankhaar, J.T. Marcus, N. Westerhof, K.M. Marques, J.G. Bronzwaer, A. Boonstra, P.E. Postmus, A. Vonk-Noordegraaf, Impaired left ventricular filling due to right-to-left ventricular interaction in patients with pulmonary arterial hypertension, Am. J. Physiol. Heart Circ. Physiol. 290 (4) (2006) H1528–H1533 (Epub November 11, 2005).
[28] J.C. Lualdi, S.Z. Goldhaber, Right ventricular dysfunction after acute pulmonary embolism: pathophysiologic factors, detection, and therapeutic implications, Am. Heart J. 130 (6) (1995) 1276–1282.
[29] Th. Desaive, S. Dutron, B. Lambermont, P. Kolh, C.E. Hann, J.G. Chase, P.C. Dauby, A. Ghuysen, Closed-loop model of the cardiovascular system including ventricular interaction and valve dynamics: application to pulmonary embolism, in: 12th International Conference on Biomedical Engineering (ICBME), Singapore, December 7–10, 2005.
[30] D. Burkhoff, T.V. Tyberg, Why does pulmonary venous pressure rise after onset of LV dysfunction: a theoretical analysis, Am. J. Physiol. Heart Circ. Physiol. 265 (1993) H1819–H1828.